Monolith Froth Reactor: Development of a Novel Three-Phase Catalytic System

Lawrence L. Crynes, Ramon L. Cerro, and Martin A. Abraham
Dept. of Chemical Engineering, The University of Tulsa, Tulsa, OK 74104

The monolith froth reactor, involving two-phase flow and a monolith catalyst, is developed. The flow within monolith channels, consisting of trains of gas bubbles and liquid slugs, is produced by forming a two-phase froth in a chamber immediately below the bottom of the monolith. The froth then flows upward into the monolith channels through pressure forces, which differs from previous methods since it may be carried out for a commercial-scale reactor. Because the liquid film which develops between the gas phase and the surface of the catalyst is extremely thin, two-phase flow within a monolith can provide reaction rates which are near their intrinsic values. Catalytic oxidation of aqueous phenol over copper oxide supported on γ-Al_2O_3 is used as a model reaction for investigating reactor performance. Generation of a froth is confirmed by visual inspection; the average bubble size is approximately that predicted by a force balance. The effect of externally controllable process variables (liquid and gas flow rates, temperature, and pressure) on the rate of phenol oxidation was investigated. Reaction rate increases with temperature or pressure increase and decreases with gas flow rate increase, achieving a maximum with respect to liquid flow rate. The activation energy calculated from the apparent reaction rate measured in the monolith froth reactor is similar to that of intrinsic value, suggesting minimal mass-transfer limitations.

Introduction

Catalysts supported on cordierite honeycomb monoliths have been increasingly used in chemical processing. Monolith supported catalysts have been used almost exclusively for gas treatment operations, most notably automotive emission exhaust control. The ceramic monolith consists of numerous small diameter, square, parallel channels through which reacting fluid can flow. A high surface area washcoat is applied to the ceramic walls to provide adequate catalyst support, and the active catalyst is impregnated onto the washcoat. Some of the advantages of the monolith support compared with more traditional pelleted catalysts include high flow rates with low pressure drop and high mechanical strength.

For three-phase chemical processes, reaction occurs on the solid surface of the catalyst. Gas must diffuse through the liquid layer to the surface of the catalyst in order for the reaction to proceed. Since the rate of diffusion through the liquid layer is generally small compared to the intrinsic rate of the chemical reaction, mass-transfer rates are important. Within the current application, the monolith support will be used to carry out a three-phase chemical reaction. In this case, the gas and liquid flow concurrently upwards through the channels of the monolith with reaction occurring on the monolith surface. It is believed that such operation should reduce the mass-transfer limitations as a result of the very thin liquid film, which is squeezed on the surface of the monolith due to gas bubbles movement.

Because the monolith consists of many small channels, it is difficult to obtain a uniform two-phase flow within the monolith channels. Mazzarino and Baldi (1992) operated a monolith reactor in both upflow and downflow configurations. During upflow operation, the liquid and gas feeds were mixed prior to the reactor and then fed through a fritted glass plate. In downflow operation, the liquid was distributed through a porous plate and the gas fed immediately above the monolith and below the porous plate. Irandoust et al. (1989) operated a three-phase monolith reactor in downflow by pulsing the liquid onto a perforated plate. Kawakami et al. (1989) obtained pulsed flow during upflow operation by placing a stainless

Correspondence concerning this article should be addressed to M. A. Abraham.

steel capillary tube into each of the channels of the monolith and the use of a peristaltic pump to feed the liquid phase.

Reviewing the use of monolith catalysts, Irandoust and Andersson (1988) describe some of the mass-transfer benefits, which may be obtained by the use of a monolith catalyst in two-phase flow. Specifically, they point out that in slug-flow operation, these systems are characterized by very efficient gas-solid and liquid-solid mass transfer. Recirculation is obtained in the liquid slugs, increasing radial mass transfer and decreasing axial dispersion. Very thin liquid films are developed on the walls of the catalyst, allowing efficient mass transfer. In experiments in single capillaries, stable films ranging in thickness less than 10 μm have been developed (Thulasidas et al., 1993). Mass-transfer rates are mainly determined by the liquid-phase diffusion coefficient, the gas liquid contact area, which is extremely high for a monolith reactor, and the length of the diffusion path, which is short in the monolith reactor.

As a result of these findings, it is expected the monolith reactors could provide apparent reaction rates near those of intrinsic kinetics. This is comparable to the performance which is obtained in a three-phase slurry reactor. The monolith reactor, however, has the advantage that the catalyst is immobilized, eliminating costly catalyst recovery steps in industrial operation. While the trickle-bed reactor provides the immobilized catalyst, a substantial price is paid in that mass-transfer rates are usually slow, and significant channeling of the gas and liquid flows may occur. Thus, the monolith three-phase reactor may be superior to either of the more traditional three-phase reactor systems, assuming that good distribution of the liquid and gas phases can be obtained in a commercially viable system.

One of the major goals of this work was to develop a mechanism by which uniform slug flow could be obtained within the monolith reactor through a feed system which could be scaled to commercial applications. To this end, a stable slug-flow pattern was generated within the monolith channels by forming a two-phase froth immediately below the monolith; the froth was fed into the channels of the monolith through pressure-driven flow. The characteristics of the gas bubbles within the froth, specifically the average bubble diameter, were controlled by varying the gas and liquid flow rates, as well as the average pore size in the fritted glass plate used to disperse the gas in the liquid layer.

This article reports on the development of the proposed three-phase reactor, in which the feed is obtained through the development of a froth immediately preceding the bottom of the monolith. The reactor was operated using the oxidation of phenol over copper oxide supported on γ-alumina as a model reaction. This reaction was chosen because of its relevance in environmental processing and its well-known kinetic behavior (Sadana and Katzer, 1974; Pintar and Levec, 1992).

We report in this article some important considerations regarding the development of this reactor. The froth region was examined for bubble size distribution. The bubble size distribution in the froth is an important parameter since it substantially controls the development of slug-flow behavior within the channels of the monolith. The aqueous phase oxidation was carried out in the novel reactor to demonstrate the validity of the reactor concept. Catalyst dissolution was seen to play a role in the performance of the reactor, and was accounted for in rate measurements. The oxidation reaction was investigated in terms of the extent of reaction and the formation of partial oxidation products. Careful attention was paid to closing the carbon balance. The apparent rate of reaction was calculated from measurement of the difference in the molar flow rate of phenol between the inlet and the outlet of the reactor and compared with measurements of intrinsic rates reported in the literature. The effects of externally controlled variables (gas and liquid flow rates, temperature and pressure) were measured to provide insight into the operation of the novel reactor. These experiments demonstrate that the monolith froth reactor, used in the configuration described, has significant potential to become a commercially viable system in which to carry out three-phase catalytic reactions.

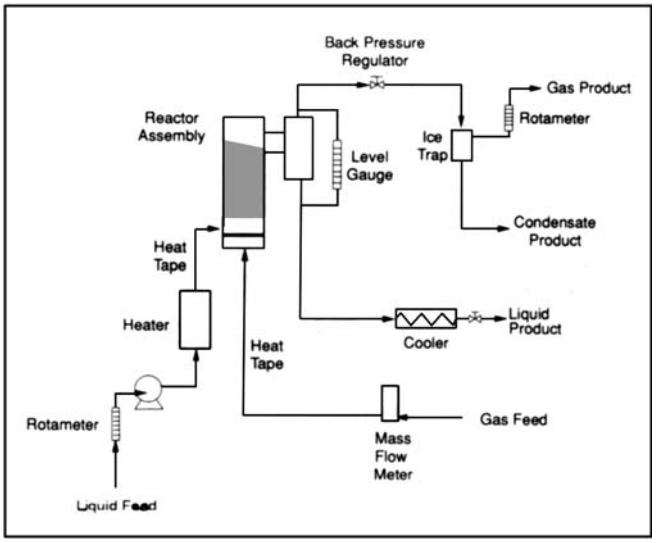

Figure 1. Monolith froth reactor experimental system indicating feed and product collection systems.

Experimental System

The full experimental system, including feed and sample collection subsystems, is shown in Figure 1. The entire system was built to a rated pressure of 600 psig at 200°C and was placed behind a 0.5-cm-thick plastic shield.

Liquid from a reservoir tank was drawn by pump suction through a high precision rotameter (Omega model FL-113) and through a diaphragm metering pump (Chem/Meter model 202V-33-115SN with steady flow cam and manifold) into the liquid heater. The heating unit was constructed from 10 cm diameter stainless steel pipe with an internal immersion heater (Chromalox MTI-240A/240); a bleed valve at the heater exit allowed removal of air during startup. Heating tape was used to maintain and control the liquid temperature in the tubing between the heater and the reactor. Temperature in the heater was controlled by feedback from a thermocouple located at the reactor entrance. The fluid pressure in the heater was monitored by mechanical gauge, and a capsu-photohelic pressure switch (Dwyer model 436004SB) was installed to turn off the heater if the pressure rose above a predetermined value. Rupture discs (3.23 MPa) were located in the liquid pump and inside the liquid heater.

Gas was fed from a high pressure cylinder, through a 40-

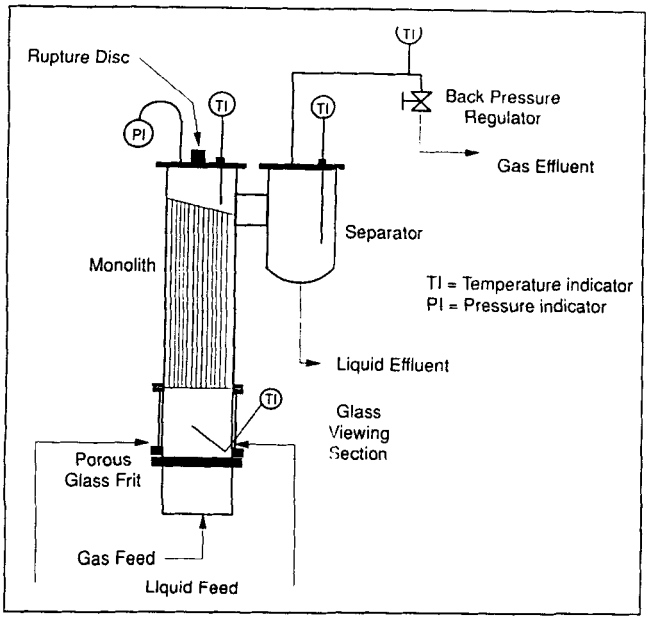

Figure 2. Monolith froth reactor.

to 50-μm filter screen then through a mass-flow meter (Omega model FMA-871-V). The gas feed stream was heated with Chromalox heating tape. Power to the heating tape was adjusted to provide a constant temperature for the gas in the feed line just prior to the reactor. A check valve was located just prior to the reactor to prevent backflow of gas through the system. Pressure was monitored by a mechanical gauge located in the gas feed line after the mass-flow meter.

The novel reactor, which forms the heart of the experimental system, was constructed in-house, and is shown in Figure 2. The lower section of the reactor was constructed of 1-cm-thick quartz which was rated to withstand pressures in excess of those used in the experimental program. Below the glass section, a porous glass disc (145- to 175-μm pore diameter) was located which allowed distribution of the gas into the liquid and the formation of a gas-liquid froth. The liquid entered the reactor from opposite sides immediately above the glass frit. The gas entered the reactor from the bottom and then passed through the fritted glass disc. A gas-liquid froth was formed above the disc which completely filled the volume immediately below the ceramic monolith. A thermocouple was located in the froth region just below the monolith.

Above the froth region, the reactor was constructed of 5-cm-dia. 304 stainless steel pipe (Sch 80). It consisted of several segments which are joined by stainless steel flanges to facilitate assembly and disassembly. The reactor length above the froth section was 0.42 m. This section of the reactor was insulated to help maintain a constant temperature along the length of the monolith. Temperature and pressure were measured in the gas space above the monolith; a high precision pressure transducer (Omega model PX612-500GV) was used for the pressure measurement. A rupture disc (3.23 MPa) was located on the top of the reactor.

The reactor section was packed with three blocks of cordierite monolith (Celcor 9475 by Corning) which were stacked within the reactor to provide a total length of 0.33 m. No alignment of the channels within the blocks was attempted. The top block was angled 15° to allow liquid to drain from the reactor into the separator. The monolith was secured within the reactor by wrapping with Fibrolax insulation, which prevented flow of the liquid and gas external to the monolith.

The gas and liquid products flow out of the reactor into a separator where the liquid is drained out the bottom and gas rises out the top. The liquid level in the separator was controlled to avoid surges of gas out the bottom of the separator. Level control was accomplished manually using a sight gauge and a fine precision metering valve. An ice-water bath was located between the separator and the metering valve to prevent flashing of the liquid as it crossed the valve. The flow rate was calculated based on the amount of liquid collected in a 10-min sample and the liquid saved for product analysis.

The gas leaving the separator passed through a back pressure regulator (GO model BP-3 102795) which was also used to control the reactor pressure. The gas was then cooled in an ice trap to remove any condensable components. The flow rate of the condensate was measured and the liquid collected for product analysis. The gas passed through a high precision rotameter (Omega model FL-114) and was then exhausted to a hood or to a gas chromatograph.

Liquid samples were analyzed using an HP 1090 liquid chromatograph with an HP ODS Hypersil, 5 μm, 100×4.6 mm column. The mobile phase was 0.01-M phosphate buffer in high-pressure liquid chromatograph (HPLC) grade water (pH adjusted to 7.0 using NaOH) plus 1% by volume of acetonitrile. The mobile phase flow rate was 1.4 mL/min, and the sample injection volume was 2.0 μm. Liquid samples were also analyzed periodically for copper and iron using a Perkin-Elmer 2380 Atomic Absorption Spectrophotometer (AAS). Gas samples were analyzed on-line using an HP 5890 gas chromatograph with a thermal conductivity detector and a Supelco 1-2390 15 ft × 1/8 in. SS 60/80 Carboxen 1000 support column.

Results

A series of experiments were performed to identify the externally adjustable parameters which have a significant role in determining the performance of the monolith froth reactor. Two distinct types of analyses were considered. First, the froth characteristics were considered important, as these determine the flow patterns which are formed within the monolith channels. Secondly, the performance of the reactor for a model reaction (aqueous phase oxidation of phenol over copper oxide) was determined.

Froth characterization

Froth behavior was analyzed using a high speed video recording system. A Kodak Ektapro EM Motion Analyzer Model 1012 with a Nikkor 55-mm microlens served as the image sensing and recording system. This processor is capable of recording images up to 1,000 full frames per second. Fiber optic back-lighting provided sufficient illumination of the image. These images were stored in a video cassette for later analysis. A Sony PVM-2530 monitor was used to display the recorded images.

Froth visualization was carried out for several operating conditions. In all cases, the feeds were brought to a steady state prior to recording the froth image. Then, images in the froth section were recorded and downloaded to the tape. A

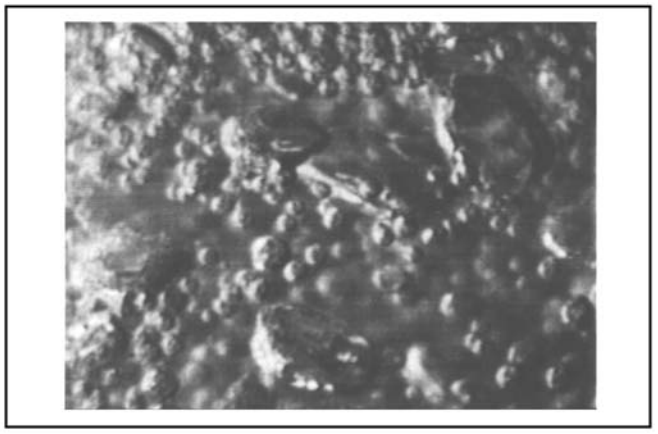

Figure 3. Froth in the reactor at 140°C, 0.91 MPa, 1.67 cm^3/s liquid flow rate, and 33.7 cm^3/s gas flow rate.

ruler was placed in the field of view to provide a scaling factor within the experimental setup and the optical system. The images are later played back at a slower rate for qualitative assessment of the shapes of the bubbles. Bubble size distribution was also obtained by measuring the sizes of all bubbles within a small section of a particular image and calibrated to the actual bubble size through the scaling factor. Reflection of light from the bubbles necessitated focus of the camera at a location near the wall of the quartz viewing section.

Figure 3 shows a photograph taken from the video recording of the froth region near the monolith entrance. The photograph indicates two different bubble sizes and shapes present in the froth. Small bubbles display a spherical shape whereas larger bubbles are primarily nonspherical. Some recirculation of gas bubbles was observed within the froth region. In all cases, a multibubble layer formed at the monolith entrance and bubbles remained in this layer for a fraction of a second before entering the monolith channels. Almost no coalescence or breakup of bubbles was observed within the froth.

Bubble size distributions (Figures 4a and 4b) were determined by measuring bubble sizes directly from the video screen and correcting for magnification effects. Experiments were conducted over a range of liquid and gas flow rates similar to those used in the reaction experiments. No effect of flow rate on bubble size distribution was observed; hence, only data from one representative set of conditions are presented in Figures 4a and 4b. The data for these figures were taken at reactor conditions of 140°C, 0.91 MPa, 1.67 cm^3/s liquid flow rate and 33.7 cm^3/s gas flow rate. The number average bubble size for these conditions was 1.40 mm with a standard deviation of 1.08 mm. Figure 4b shows that, although fewer in number, the larger bubbles account for the majority of the volumetric gas flow.

The observed number average bubble size in the froth can be compared with that expected from fluid mechanical considerations. A force balance on the gas bubble as it passes through the gas frit provides:

$$d_b = \left(\frac{6\sigma d_0}{g(\rho_L - \rho_G)}\right)^{1/3} \tag{1}$$

The maximum pore size in the glass frit is 175 μm, which results in a calculated bubble diameter of 1.87 mm. This value is slightly above the average diameter observed by high speed video. Pores smaller than 175 μm would produce bubbles smaller than that estimated by Eq. 1 and could account for the smaller bubbles observed by video. Coalescence of bubbles during formation could occur due to the closeness of pores in the frit and would account for bubbles larger than estimated. The effect of gas flow rate could also have some effect on bubble size.

Greater than 90% of the gas volume is present as bubbles with a diameter approximately equal to or above the monolith channel dimension of 1.27 mm. Also, no breakup of gas bubbles was observed within the froth region. In order for these large bubbles to enter the monolith channels without breaking apart, the diameter must be squeezed into the channel diameter (or slightly smaller) and the bubble elongated. Liquid slugs enter the monolith channels interspersed with the gas bubbles. This process produces slug flow within the channels of the

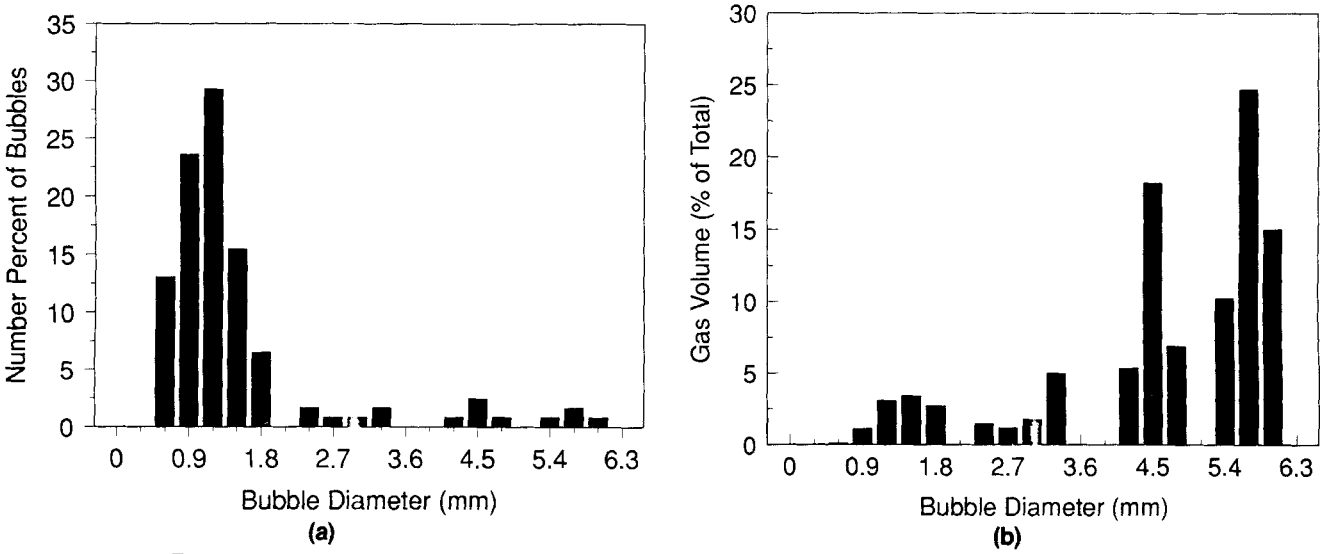

Figure 4. (a) Bubble size distribution and (b) bubble volume distribution in the froth.

At 140°C, 0.91 MPa, 1.67 cm^3/s liquid flow rate, and 33.7 cm^3/s gas flow rate.

Table 1. Monolith Specifications: Celcor 9475 by Corning

Cordierite Ceramic (Magnesium Aluminosilicate)		
Square Cell Geometry:		
Number of Cells: 400 channels/in.		
Cell Dimension: 1.27 mm		
Wall Thickness: 0.15 mm		
Density: 384.451 kg/m^3		
Geometric Surface Area: 2.755 mm^2/mm^3		
Hydraulic Diameter: 1.12 mm		
Open Frontal Area: 77%		
Properties of Gamma Alumina and Cordierite:		
	γ-Al_2O_3	Cordierite
Surface Area	3.65×10^3 m^2/kg	2.59×10^3 m^2/kg

monolith. In order to control the bubble size within the channels, it is necessary to control the bubble size within the froth region. An increase in the average bubble size could produce improved slug flow operation within the monolith channels. As seen from Eq. 1, the froth bubble size could be increased independently of any other parameters by increasing the pore diameter of the fritted glass disc.

Reaction experiments

The analysis of reactor performance was determined in terms of the aqueous phase oxidation of phenol over a CuO catalyst. The experimental procedures are described first, and then some overall performance observations, including the formation of partial oxidation products and the stability of the catalyst, are presented. Finally, the effects of externally adjustable process variables on the measured rate of reaction are described.

Experimental Procedures. Experiments have been conducted to study the effects of process variables on reaction rates and reaction products. Aqueous phenol was prepared by dissolving phenol (Aldrich) into Millipore purified water to obtain a 5,000 ppm solution. Breathing air was used as the source of oxygen. A γ-Al_2O_3 washcoat was applied to the monolith by Allied Signal Environmental Catalysts, Tulsa, OK upon which the CuO catalyst was impregnated. The CuO loading was 23.1 kg/m^3. Monolith specifications are given in Table 1. The reactor was operated in steady-state, concurrent upflow. The temperature difference from monolith bottom to top was $\leq \pm 2$°C.

Experiments were performed according to the following procedures. Gas flow was started first, to keep liquid from passing into the chamber below the glass frit. After the gas flow was adjusted to the desired set point, liquid flow was initiated and brought to the set point value. Heating of both liquid and gas feeds were accomplished in a temperature ramp, increasing 10–15°C/min until the set point values were reached. The pressure was then adjusted to the set point value. After all the set points were reached, the reactor was operated for approximately 1 h to ensure steady-state operation. During operation, the exit flow rate of the liquid was adjusted to maintain an approximately constant level in the separator. Also, the liquid product exit flow rate needed to be adjusted whenever the temperature or pressure was changed.

Product samples were obtained on a periodic basis. Two samples were taken for each reaction condition. After changing a process variable to a new set point value, 30 to 60 min was allowed to elapse to ensure that steady state was achieved.

Table 2. Experimental Conditions

Liquid Flow Rate	0.4 to 3.5 cm^3/s
Gas Flow Rate	15.8 to 50 cm^3/s
Temperature	110 to 150°C
Pressure	0.48 to 1.17 MPa

Liquid samples were collected over a 10 to 30 min time period; the amount of sample collected was recorded and measured as the liquid flow rate. Care was taken to ensure that the liquid level in the separator remained constant during the sampling period. Liquid condensate was measured over a 10 min time period to collect sufficient liquid for later analysis. Gas samples were sent directly to the gas chromatograph. All liquid samples which were collected were stored for later HPLC analysis.

The amount of phenol consumed by reaction was determined using HPLC analysis of the liquid feed and products. Reaction rate was calculated according to the change in flow rate of phenol:

$$-r_{ph} = \frac{F_{ph,in} - F_{ph,out}}{W_{cat}} \tag{2}$$

The molar flow rates of phenol, $F_{ph,in}$ and $F_{ph,out}$, were determined from the measured volumetric flow rates of the liquids and the concentration of phenol in these liquids, as determined by HPLC analysis.

Initially, experiments were planned with a factorial design. However, proposed operating conditions, which were within the limitations of the experimental equipment, could not be obtained in practice. Experimental conditions are given in Table 2. Difficulties included excessive vaporization of the liquid feed into the gas phase, excessive moisture carryover into the gas product, and inability to obtain the desired operating temperature with the available heating system. Because of these difficulties, the factorial design could not be completed. However, a complete set of reaction rate data was obtained for each of the externally controllable variables (liquid and gas flow rates, temperature, and pressure) at constant values of the other variables. Presently, a total of 37 runs have been conducted, several of which provide replicate data for identical operating conditions. The plots presented in the following figures contain averaged data when replicate runs were available.

Experimental error was estimated by considering the maximum error inherent in each measurement involved in the reaction rate calculation. The experimental measurement of reaction rate was taken according to Eq. 2. The error associated with this calculation represents a combination of the errors associated with each individual measurement,

$$\delta(-r_{ph}) = \left|\frac{\partial(-r_{ph})}{\partial F_{ph,in}}\delta F_{ph,in}\right| + \left|\frac{\partial(-r_{ph})}{\partial F_{ph,out}}\delta F_{ph,out}\right| + \left|\frac{\partial(-r_{ph})}{\partial W_{cat}}\delta W_{cat}\right| \tag{3}$$

where δF represents the error in the flow rate measurement and δW represents the error in the measurement of catalyst weight (Bragg, 1974). The catalyst weight is determined by subtracting the amount of catalyst lost from the initial catalyst loading. Catalyst loss calculations involve measurement of the

liquid exit flow rate, dilution of a liquid product sample and concentration measurements by AAS, as described later. The error estimated for the reaction rate according to Eq. 3 is approximately 0.5 mol/(g cat)(s), depending upon the specific conditions under which the run was carried out. This value is large compared to many of the rate measurements, however, it is smaller than the order of magnitude changes which are observed as the process variables are varied. The measured conversion from replicate runs taken under identical process conditions always remained less than the expected error calculated by Eq. 3.

One of the major factors affecting the error calculation is the large relative error associated with the measurement of phenol conversion by concentration measurements with the HPLC. While the measurement of concentration is accurate to within a few percent, the rate calculation represents the difference between two concentration measurements. This difference is generally less than 5%. Thus, the error in the HPLC concentration measurement is large compared to the difference in the measurements of the inlet and outlet phenol concentration.

Overall Performance Observations. The complete combustion of phenol can be described by the following equation:

$$C_6H_5OH + 7O_2 \rightarrow 6CO_2 + 3H_2O \qquad (4)$$

The major reaction product observed from the monolith reactor was CO_2. Possible minor products indicated by other researchers include: p-benzoquinone, o-benzoquinone, benzenediole, hydroquinone, catechol and organic acids (Devlin and Harris, 1984; Pintar and Levec, 1992b; Sadana and Katzer, 1974a,b); trace amounts of these products were indicated by HPLC analysis. Changes in the color of reactor products from clear to a yellow/brown also indicated the presence of p-benzoquinone and o-benzoquinone as noted by other investigators for conversions below about 60% (Sadana and Katzer, 1974b). In other research, polymeric products have also been observed and have contributed to catalyst deactivation (Pintar and Levec, 1992b). No such products were found in our studies.

Closure of the carbon mole balance was checked based on the assumption of complete combustion, as outlined by Eq. 4. Analyzing all liquid streams for phenol concentration and the gas stream for CO_2 allowed closure of the mole balance:

$$\frac{C_{out}}{C_{in}} = \frac{6F_{ph,out} + F_{CO_2}}{6F_{ph,in}} \qquad (5)$$

to within 10% for most runs. Because the concentration of partial oxidation products was always small, inclusion of the carbon which was present in these materials did not substantially alter the closure of the material balance.

AAS analysis of periodic liquid samples revealed copper in the product samples. Analysis of feed samples showed no copper. The only source for copper was the CuO catalyst. Although the amount of copper loss was a function of operating conditions, total copper loss from the monolith was estimated to be 2.1×10^{-3} kg after approximately 50 h of run time. This corresponds to a loss of 20% of the initial loading. Possible causes of copper loss include dissolution in the hot acidic aqueous phase or erosion due to the flow within a monolith

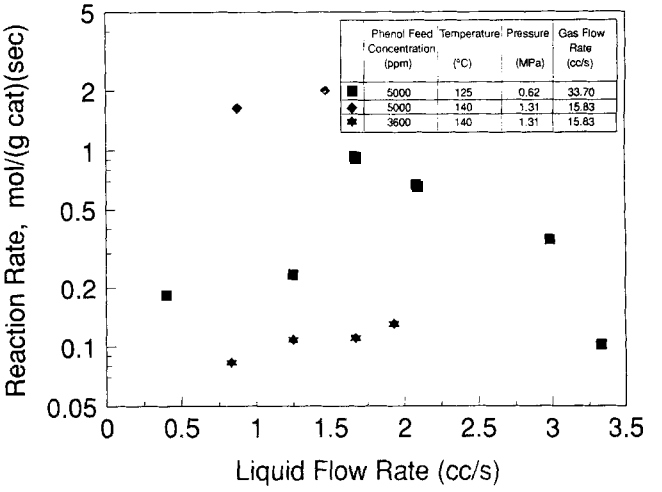

Figure 5. Effect of liquid flow rate on the overall reaction rate at different fixed gas flow rate, temperature, and pressure.

channel (Pintar and Levec, 1992b). In all calculations which follow, the reaction rate has been based on the actual copper concentration on the catalyst at the time of the experiment.

Effect of Externally Adjustable Process Variables on Reaction Rate. The effect of liquid flow rate on reaction rate (as calculated by Eq. 2) is shown in Figure 5, with data obtained at two different reaction temperatures and two different phenol concentrations. The most extensive data was obtained at 5,000 ppm and 125°C. At this condition, a maximum in reaction rate was observed at a liquid flow rate of about 1.7 cm^3/s. At the higher temperature, and independent of concentration, the rate of reaction was seen to increase as the liquid flow rate increased; however, the liquid flow rates were less than 2 cm^3/s at this temperature. Comparison of the 140°C data reveals that increasing phenol concentration led to an increase in the observed reaction rate.

Figure 6 indicates the effect of gas flow rate on the observed reaction rate. In all cases, the reaction rate decreases slightly

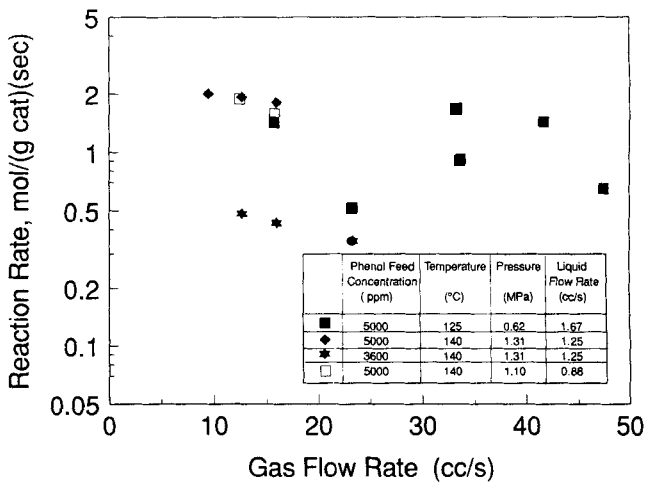

Figure 6. Effect of gas flow rate on the overall reaction rate at different fixed liquid flow rate, temperature, and pressure.

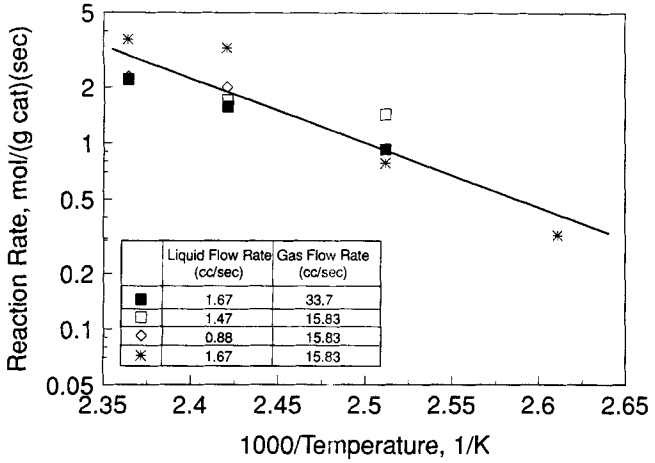

Figure 7. Effect of temperature on the overall reaction rate at different fixed liquid and gas flow rates, and pressure.

as gas flow increases. The data obtained at 5,000 ppm and 125°C has substantial scatter, since it represents the results of several experiments performed over a large time interval. Consideration of catalyst deactivation, minor variations in analytical procedures, modifications in flow measurement equipment, and other experimental variables were not controlled carefully throughout this period. Despite this, the data matches well with other data available under similar conditions and provides a set of data which is internally consistent.

The observed decrease in reaction rate as the gas flow rate increases could simply be a result of changes in the volume available for liquid flow. As the gas flow rate increases, the gas occupies a larger volume within the reactor, leaving less volume available for the liquid. Since the liquid flow rate remains unchanged, the residence time of the liquid phase is decreased as the gas flow rate increases. Thus, phenol has less time in which it is in contact with the catalyst and the phenol conversion would decrease. A decrease in conversion at a constant liquid flow rate corresponds to a decrease in the measured reaction rate, according to Eq. 2, as observed experimentally. Additional effects, including changes in the mass-transfer performance, could occur as the gas flow rate is increased.

The effect of temperature on reaction rate is indicated in Figure 7, which reports the data in Arrhenius fashion (log rate vs. $1/T$). Clearly, reaction rate increased as the reaction temperature increased. The straight line in Figure 7 represents the best fit line for all of the experimental data taken in this study. The data shown are for constant volumetric gas flow rate; therefore, no effect of temperature on flow regimes should exist. However, reactor pressure was increased as temperature was increased to avoid boiling the aqueous phenol. Therefore, the molar flow rate of air had to be increased to maintain the same volumetric flow rate within the reactor.

According to normal kinetics analysis, the reaction rate is related to the phenol concentration as:

$$-r_{ph} = kf(C_{ph}, C_{O_2}, C_i) \qquad (6)$$

where C_i represents the concentration of all components other than oxygen and phenol, which are accounted for explicitly. Since all of the data in Figure 7 were obtained at identical

Table 3. Apparent Activation Energies

Activation Energy kJ/mol	Reference
66.9	This study
25.1	Monolith Froth Reactor (Kim, 1991)
83.7	Intrinsic/Slurry reactor (Pintar and Levec, 1992b)
175.7	Intrinsic/Slurry reactor (Sadana and Katzer, 1974b)
276.2	Initial activity regime/Intrinsic/Slurry reactor (Sadana and Katzer, 1974b)
41.8	Vapor phase reactor (Walsh and Katzer, 1973)

concentration conditions, the only temperature dependent variable is the rate constant, k. In these experiments, the conversion was always less than approximately 10%, and the assumption of a differential reactor (constant concentrations) apply. Under these conditions, the rate constant is related to the temperature by the activation energy, which is the slope of the straight line indicated in Figure 7. The value calculated in this case was 67 kJ/mol, which compares favorably with other values in the literature and indicated in Table 3. Indeed, this value is only slightly less than the intrinsic value of 83.7 kJ/mol reported recently by Pintar and Levec (1992b). This result suggests that the rate observed in the current reactor is close to the intrinsic reaction rate and is only slightly inhibited by mass-transfer limitations.

The effect of pressure on reaction rate is shown in Figure 8 for three different sets of experimental conditions, but at constant molar gas flow rate. Maintaining a constant molar gas flow rate while increasing pressure results in a decrease in the volumetric flow rate of the gas due to its compressibility. As previously noted in Figure 6, reaction rate increases as volumetric gas flow rate decreases; this could account for the observed increase in reaction rate as pressure increases. However, the increase in reaction rate with increasing pressure could also be explained based on an increased solubility of oxygen in the aqueous phase with increased pressure. Thus, the concentration of oxygen in the liquid phase would increase. If mass-transfer considerations are important, increasing the oxygen concentration at the gas-liquid interface will increase the

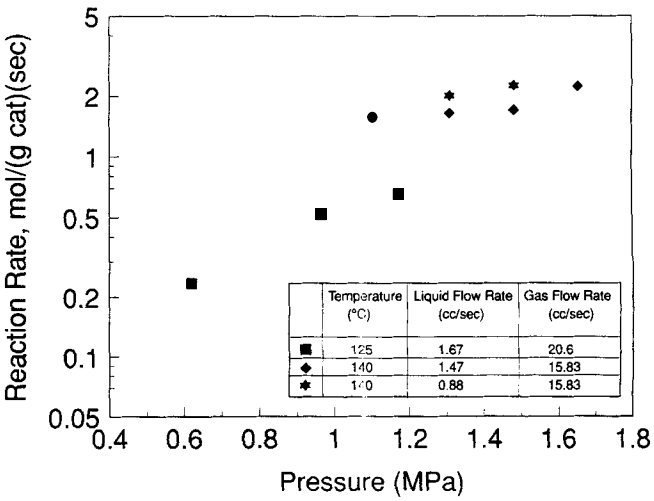

Figure 8. Effect of pressure on the overall reaction rate at different fixed liquid and gas flow rates, and temperature.

driving force for mass transfer through the liquid film, resulting in a higher concentration of oxygen at the catalyst surface. For positive order kinetics, an increased concentration at the catalyst surface would provide a higher reaction rate. Thus, operation at higher pressure should enhance reaction rate, as observed.

Discussion

Within the monolith froth reactor, each of the externally controllable variables, namely liquid and gas flow rates, pressure and temperature, can affect many internally important parameters, which in turn leads to significant variation in the performance of the reactor. Some of the primary effects of changing the externally controllable variables include changing the residence time of the liquid phase within the reactor, changing the mass-transfer characteristics, and complete shift in the flow regime within the monolith channels. To complicate matters, the effects of the externally controllable variables are interconnected. For example, the gas density will be decreased by increasing the reaction temperature, but may be returned to its original value by increasing the reactor pressure. However, each of these changes in temperature and pressure also impact the rate of mass transfer, the solubility of oxygen in the liquid phase, and the intrinsic rate of the chemical reaction.

The rate of mass transfer through the liquid film to the catalyst wall is important in determining the observed reaction rate. Unless intrinsic reaction kinetics can be obtained, the mass-transfer rate will control the observed reaction rate within the reactor. Intrinsic kinetics are obtained only in the situation where the rate of mass transfer is much greater than the rate of chemical reaction on the surface of the catalyst. By changing the liquid and gas flow rates, the proportion of liquid in the slug compared with that in the film changes. Since the rate of mass transfer within the slugs would be expected to be different from that in the film, it would be expected that changing the liquid and gas flow rates should change the mass-transfer rates per unit volume of the reactor. However, Irandoust et al. (1992) report that the influence of flow rate is only secondary in determining mass-transfer properties within the channels of the monolith. On the contrary, preliminary experiments and a detailed analysis of the hydrodynamics of trains of bubbles and liquid slugs (Thulasidas et al., 1994) points to a mass-transfer process clearly dependent on the liquid flow properties. Increasing temperature would provide higher values for the diffusion coefficient but lower values for the solubility of oxygen in the liquid phase. Thus, the effect of temperature on the mass-transfer rate is also obscure.

Since the liquid residence time is inversely related to the liquid flow rate, it must decrease as the liquid flow rate increases. This indicates that conversion should decrease as the liquid flow rate increases. Now, for a fixed catalyst weight, the reaction rate is proportional to $(F_{ph,in}X)$, where X is the phenol conversion. Combining these conditions reveals that the reaction rate may be expected not to vary substantially as the liquid flow rate changes. However, the reaction rate, as measured by the concentration and residence time, also must include a term which converts from the volume of the reactor to the volume of liquid within the reactor, $\phi = V_{liq}/V_{rxr}$. Making this conversion transforms Eq. 2 as:

$$-r_{ph} = \frac{C_{A,in}X}{\tau\phi\rho_{cat}} \tag{7}$$

Thus, the reaction rate turns out to be dependent on both the liquid and gas flow rates through the liquid volume fraction. It would be tempting to suggest that the liquid volume fraction is strictly the ratio of the liquid flow rate to the total flow rate, but experimental evidence (Patrick et al., 1994) reveals that this is not the case.

The reaction rate was seen to increase as the liquid flow rate increased under some conditions, but decrease with increasing liquid flow rate under other conditions (Figure 5). This is an example of the complex role of the externally controllable parameters on the internal variables which determine the reaction rate. Increasing the liquid flow rate increases ϕ, the volume fraction of the liquid phase relative to the total volume. If the ratio of conversion over residence time (X/τ) remains approximately constant, Eq. 7 predicts that an increase in the liquid flow rate should lead to a decrease in the reaction rate, as observed for high liquid flow rates.

In addition to the effects of the externally controllable variables on the values of the parameters within the monolith, these variables will also dictate the flow regime which is present within the monolith channels. It is well-known, and has previously been reported (Kim, 1989), that two-phase flow may exist as bubble flow, slug flow, or annular flow. Clearly, each of these flow regimes will have different performance characteristics. At low liquid flow rates, the rate of reaction was seen to increase as the liquid flow rate increases. This could be a result of changing flow regime within the monolith channels as the liquid flow rate is increased. At very low liquid flow rates, the gas volume is much greater than the liquid volume and gas channeling might prevail within the monolith channels. Gas channeling would yield relatively low reaction rates. As the liquid flow rate increases, a greater percentage of the monolith channels may exhibit slug-flow behavior, thereby increasing the observed reaction rate.

The bubble size within the froth is one parameter useful in predicting the flow regime, which will be present within the monolith channels. While the gas and liquid flow rates have only a minor impact on the bubble size, the temperature and pressure will influence the average bubble size within the froth. According to Eq. 1, the average bubble size will be increased by increasing the surface tension or decreasing the density difference between the gas and the liquid phase. These two parameters are impacted by temperature and the density difference is impacted by pressure. Thus the flow regime within the monolith channels is affected by changes in temperature and pressure through the average bubble size in the froth.

Conclusion

A novel three-phase reactor has been developed which takes advantage of the flow properties of a two-phase system within the channels of a ceramic monolith. During cocurrent upflow, bubble train flow, consisting of sequential slugs of liquid and gas bubbles, is developed. The liquid within the slugs is well mixed and the liquid films on the catalyst wall during the passing of a gas bubble are extremely thin. This combination of flow characteristics leads to very high mass-transfer rates, resulting in observed reaction rates near their intrinsic values.

The bubble train flow within the monolith channels was obtained by the formation of a froth in a chamber immediately below the monolith. The two-phase mixture proceeds into the channels of the monolith by pressure forces. The average bubble diameter is most significantly a function of the pore size in the fritted glass through which the gas must proceed; this bubble size must be larger than the monolith channel diameter in order to produce bubble train flow. Because a froth may be formed in a large diameter chamber, this method of producing a bubble train flow within a monolith is commercially viable.

Oxidation of aqueous phenol over a CuO catalyst was used as a model reaction for investigating reactor performance. The observed rate of reaction was found to increase as temperature or pressure increased and to decrease slightly as gas flow rate increased. Reaction rate showed a maximum with respect to liquid flow rate at about 1.7 cm^3/s. The data permitted calculation of an activation energy, which was only slightly below that reported in the literature as the intrinsic value, suggesting that mass-transfer limitations are minimal in the monolith froth reactor.

Acknowledgments

The authors are grateful to the National Science Foundation (NSF Grant CTS-9022241) and the U.S. Department of Energy-Energy Research Traineeship program for support of this work, and to Allied Signal Environmental Catalysts for catalyst preparation.

Notation

C_{out}/C_{in} = ratio of carbon out of the reactor to carbon into the reactor
d_b = bubble diameter, m
d_o = pore diameter in the frit, m
$F_{ph,in}$ = molar flow rate of phenol into the reactor, mol/s
$F_{ph,out}$ = molar flow rate of phenol out of the reactor, mol/s
g = acceleration due to gravity, m/s^2
F_{CO_2} = molar flow rate of CO_2 out of the reactor, mol/s
MW_{ph} = molecular weight of phenol
$-r_{ph}$ = rate of phenol disappearance, mol/kg·s
W_{cat} = weight of catalyst in the reactor, kg

Greek letters

ρ_G = gas density, kg/m^3
ρ_L = aqueous phase density, kg/m^3
σ = aqueous phase surface tension, N/m
τ = residence time of the liquid phase in the monolith froth reactor, s
ϕ = liquid volume fraction within the monolith froth reactor

Literature Cited

Ariga, O., M. Kimura, M. Taya, and T. Kobayashi, "Kinetic Evaluation and Characterization of Ceramic Honeycomb-Monolith Bioreactor," *Ferment. Tech.*, **64**, 327 (1986).

Benoit, M. R., and J. T. Kohler, "An Evaluation of a Ceramic Monolith as an Enzyme Support Material," *Biotech. Bioeng.*, **XVII**, 1617 (1975).

Borkawski, B., "The Catalytic Oxidation of Phenols and Other Impurities in Evaporated Effluents," *Water Res.*, **1**, 367 (1967).

Bragg, G., *Principles of Experimentation and Measurement*, Prentice-Hall, Englewood Cliffs, NJ, p. 95 (1974).

Devlin, H. R., and I. J. Harris, "Mechanism of the Oxidation of Aqueous Phenol with Dissolved Oxygen," *Ind. Eng. Chem. Fundam.*, **23**, 387 (1984).

Hatziantoniou, V., and B. Andersson, "The Segmented Two-Phase Flow Monolithic Catalyst Reactor. An Alternative for Liquid-Phase Hydrogenations," *Ind. Eng. Chem. Fundam.*, **23**, 82 (1984).

Irandoust, S., and B. Andersson, "Mass Transfer and Liquid-Phase Reactions in a Segmented Two-Phase Flow Monolithic Catalyst Reactor," *Chem. Eng. Sci.*, **43**, 1983 (1988).

Kawakami, K., K. Kawasaki, F. Shiraishi, and L. Lusunoki, "Performance of a Honeycomb Monolith Bioreactor in a Gas-Liquid-Solid Three-Phase System," *Ind. Eng. Chem. Res.*, **28**, 394 (1989).

Kim, S., "Three-Phase Catalytic Oxidation of Phenol in a Monolithic Reactor," MS Thesis, Univ. of Tulsa, Tulsa (1991).

Mazzarino, I., and G. Baldi, "Liquid Phase Hydrogenation on a Monolithic Catalyst," in *Recent Trends in Chemical Reaction Engineering*, B. D. Kulkarni, R. A. Mashelkar, and M. M. Sharma, eds., Vol. 2, Wiley Eastern Limited, Bombay, India, p. 181 (1992).

Patrick, R. H., Jr., T. Klindera, L. L. Crynes, R. L. Cerro, and M. A. Abraham, "Residence Time Distribution in a Three-Phase Monolith Reactor," *AIChE J.*, in press (1995).

Pintar, A., and J. Levec, "Catalytic Liquid-Phase Oxidation of Refractory Organics in Waste Water," *Chem. Eng. Sci.*, **47**, 2395 (1992a).

Pintar, A., and J. Levec, "Catalytic Oxidation of Organics in Aqueous Solutions," *J. Catal.*, **135**, 345 (1992b).

Sadana, A., and J. R. Katzer, "Involvement of Free Radicals in the Aqueous Phase Catalytic Oxidation of Phenol Over Copper Oxide," *J. Catal.*, **35**, 140 (1974a).

Sadana, A., and J. R. Katzer, "Catalytic Oxidation of Phenol in Aqueous Solution over Copper Oxide," *Ind. Eng. Chem. Fundam.*, **13**, 127 (1974b).

Satterfield, C. N., and F. Ozel, "Some Characteristics of Two-Phase Flow in Monolithic Catalyst Structure," *Ind. Eng. Chem. Fundam.*, **16**, 61 (1977).

Thulasidas, T. C., M. A. Abraham, and R. L. Cerro, "Bubble-Train Flow in Capillaries of Circular and Square Cross Section," *Chem. Eng. Sci.*, **49** (1994).

Walsh, M., and J. Katzer, "Catalytic Oxidation of Phenol in Dilute Concentration in Air," *Ind. Eng. Chem. Process Des. Develop.*, **12**(4), 477 (1973).

Manuscript received Nov. 4, 1993, and revision received Feb. 23, 1994.